Inorganic Chemistry
Article

Inorg. Chem. **2010**, *49*, 10875–10881 **10875**
DOI: 10.1021/ic101221z

Controlled Sulfur Oxygenation of the Ruthenium Dithiolate (4,7-Bis-(2′-methyl-2′-mercaptopropyl)-1-thia-4,7-diazacyclononane)$RuPPh_3$ under Limiting O_2 Conditions Yields Thiolato/Sulfinato, Sulfenato/Sulfinato, and Bis-Sulfinato Derivatives

César A. Masitas, Manoj Kumar, Mark S. Mashuta, Pawel M. Kozlowski, and Craig A. Grapperhaus*

Department of Chemistry, University of Louisville, Louisville, Kentucky 40292, United States

Received June 18, 2010

The ruthenium(II) dithiolate complex (bmmp-TASN)$RuPPh_3$ (**1**) reacts with O_2 under limiting conditions to yield isolable sulfur oxygenated derivatives as a function of reaction time. With this approach, a family of sulfur−oxygenates has been prepared and isolated without the need for O-atom transfer agents or column chromatography. Addition of 5 equiv of O_2 to **1** yields the thiolato/sulfinato complex (bmmp-O_2-TASN)$RuPPh_3$ (**2**) in 70% yield within 5 min. Increasing the reaction time to 12 h yields the sulfenato/sulfinato derivative (bmmp-O_3-TASN)$RuPPh_3$ (**3**) in 82% yield. Longer reaction times and/or additional O_2 exposure yield the bis-sulfinato complex (bmmp-O_4-TASN)$RuPPh_3$ (**4**). All products remain in the Ru(II) oxidation state under the conditions employed. Stoichiometric hydrolysis of acetonitrile to acetamide by **2** and **3** is observed in mixed acetonitrile, methanol, PIPES buffer (pH = 7.0) mixtures. The Ru(III)/(II) reduction potential of −0.85 V (versus ferrocenium/ferrocene) for **1** shifts to −0.39 and −0.26 V for **2** and **3**, respectively, because of the decreased donor ability of sulfur upon oxygenation. X-ray diffraction studies reveal a decrease in Ru−S bond distances upon oxygenation by 0.045(1) and 0.158(1) Å for the sulfenato and sulfinato donors, respectively. Conversely, sulfur−oxygenation increases the Ru−P bond distance by 0.061(1) Å from **1** to **2** and an additional 0.027(1) Å from **2** to **3**. Density functional theory investigations using the BP86 and B3LYP functionals with a LANL2DZ basis set for Ru and the 6-31G(d) basis set for all other atoms reveal a direct correlation between the oxygenation level and the Ru−P distance with an increase of 0.031 Å per O-atom.

Introduction

The hydrolytic metalloenzymes nitrile hydratase (NHase) and thiocyanate hydrolase (SCNase) share an uncommon post-translational modification.[1−6] Metal-coordinated thiolates in these enzymes react with dioxygen to yield sulfur-oxygenated derivatives as a prerequisite for catalytic activity. The active site of NHase contains a low-spin Fe(III) or Co(III) in an N_2S_3 donor set composed of two carboxamido nitrogen donors and three cysteine derived sulfurs, Figure 1. Two of the cysteine thiolates have been oxygenated resulting in the unusual thiolato (RS^-), sulfenato (RSO^-), sulfinato (RSO_2^-) donor combination that is also observed at the Co(III) active site of SCNase.[1−3] The sulfur-oxygenated ligands have been proposed to modulate the Lewis acidity of the metal center, serve as a proximal base during turnover, and/or modify substrate/product/inhibitor binding affinity.[3−8] A number of small molecule active site mimics have been prepared to help delineate these proposed roles and the sulfur−oxygenation pathway.[9−21]

*To whom correspondence should be addressed. E-mail: grapperhaus@louisville.edu.

(1) Shigehiro, S.; Nakasako, M.; Dohmae, N.; Tsujimura, M.; Tokoi, K.; Odaka, M.; Yohda, M.; Kamiya, N.; Endo, I. *Nat. Struct. Mol. Biol.* **1998**, *5*, 347–351.
(2) Miyanaga, A.; Fushinobu, S.; Ito, K.; Wakagi, T. *Biochem. Biophys. Res. Commun.* **2001**, *288*, 1169–1174.
(3) Arakawa, T.; Kawano, Y.; Kataoka, S.; Katayama, Y.; Kamiya, N.; Yohda, M.; Odaka, M. *J. Mol. Biol.* **2007**, *366*, 1497–1509.
(4) Endo, I.; Odaka, M.; Yohda, M. *Trends Biotechnol.* **1999**, *17*, 244–249.
(5) Murakami, T.; Nojiri, M.; Nakayama, H.; Odaka, M.; Yohda, M.; Dohmae, N.; Takio, K.; Nagamune, T.; Endo, I. *Protein Sci.* **2000**, *9*, 1024–1030.
(6) Arakawa, T.; Kawano, Y.; Katayama, Y.; Nakayama, H.; Dohmae, N.; Yohda, M.; Odaka, M. *J. Am. Chem. Soc.* **2009**, *131*, 14838–14843.
(7) Noguchi, T.; Honda, J.; Nagamune, T.; Sasabe, H.; Inoue, Y.; Endo, I. *FEBS Lett.* **1995**, *358*, 9–12.
(8) Tsujimura, M.; Odaka, M.; Nagashima, S.; Yohda, M.; Endo, I. *J. Biochem.* **1996**, *119*, 407–413.
(9) Grapperhaus, C. A.; Patra, A. K.; Mashuta, M. S. *Inorg. Chem.* **2002**, *41*, 1039–1041.
(10) Grapperhaus, C. A.; Li, M.; Patra, A. K.; Poturovic, S.; Kozlowski, P. M.; Zgierski, M. Z.; Mashuta, M. S. *Inorg. Chem.* **2003**, *42*, 4382–4388.
(11) O'Toole, M. G.; Bennett, B.; Mashuta, M. S.; Grapperhaus, C. A. *Inorg. Chem.* **2009**, *48*, 2300–2308.
(12) O'Toole, M. G.; Kreso, M.; Kozlowski, P. M.; Mashuta, M. S.; Grapperhaus, C. A. *J. Biol. Inorg. Chem.* **2008**, *13*, 1219–1230.
(13) Kung, I.; Schweitzer, D.; Shearer, J.; Taylor, W. D.; Jackson, H. L.; Lovell, S.; Kovacs, J. A. *J. Am. Chem. Soc.* **2000**, *122*, 8299–8300.
(14) Kovacs, J. A. *Chem. Rev.* **2004**, *104*, 825–848.

Published on Web 10/26/2010

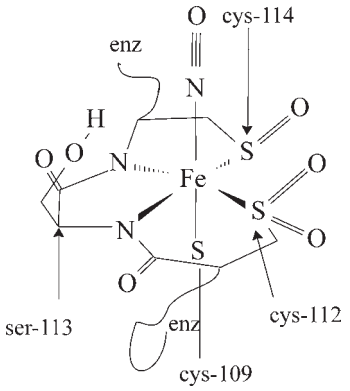

Figure 1. Active site of Fe-containing NHase.

The typical approach to prepare sulfur-oxygenated mimics of NHase or SCNase involves the reaction of metal−thiolate precursors with O-atom transfer agents such as H_2O_2, *N*-sulfonyloxaziridine, (1*S*)-(+)-(10-camphorsulfonyl)oxaziridine, or urea hydrogen peroxide.[13,15,17,20−22] These efforts have been successful for the isolation of sulfenato,[15,17,21,22] sulfinato,[17,20] and a mixed sulfenato/sulfinato complex with η^2-sulfenate coordination.[13] A major advantage of O-atom transfer agents is the ability to quantitatively add oxidizing equivalents at controlled rates. Less well developed are reactions employing dioxygen, which is the proposed reagent in the enzymatic systems.[2,5,6] While several sulfinato complexes have been reported upon O_2 exposure of thiolate precursors,[13,23−32] isolation of sulfenato[25,33] or mixed sulfenato/sulfinato complexes from O_2 are rare.[34−36]

Scheme 1. Oxygenation Pathways of **1**

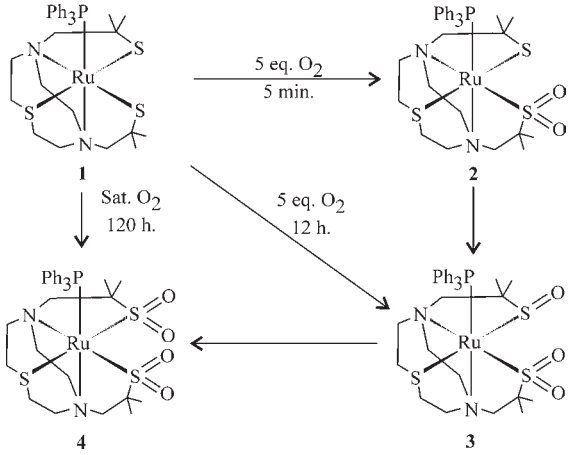

Previously, our laboratory has focused on NHase model complexes based on the N_2S_3 chelate 4,7-bis-(2′-methyl-2′-mercaptopropyl)-1-thia-4,7-diazacyclononane (bmmp-TASN).[9−12] With this ligand, a series of iron complexes was synthesized, and their oxygen sensitivity was investigated.[10] Oxygen exposure of the high-spin complex (bmmp-TASN)-FeCl yields ligand disulfide with decomplexation of the metal and subsequent iron-oxo cluster formation.[37] In contrast, O_2 addition to the low-spin complex (bmmp-TASN)FeCN generates the bis-sulfonato (2 RSO_3^-) complex (bmmp-O_6-TASN)FeCN.[12] While the low-spin complex promoted sulfur oxygenation, the reaction proceeded beyond the oxygenation level observed in NHase and SCNase. On the basis of these initial results, we recently communicated the synthesis of (bmmp-TASN)RuPPh$_3$ (**1**) and its reactivity under limited O_2 conditions to yield the mixed sulfenato/sulfinato complex (bmmp-O_3-TASN)RuPPh$_3$ (**3**).[34] Herein we report additional studies under limited O_2 conditions. By fixing the quantity of O_2 and the duration of the reaction, conditions were optimized to reproducibly obtain the monosulfinato (bmmp-O_2-TASN)-RuPPh$_3$ (**2**) and bissulfinato (bmmp-O_4-TASN)RuPPh$_3$ (**4**) derivatives without the need for O-atom transfer reagents or purification by column chromatography. This approach has yielded a unique "family" of complexes, **1**−**4**, that differ only in the degree of S-oxygenation, Scheme 1. Although the number of reported S-oxygenates is growing, families containing three or more oxygenated derivatives are scant.[38,39] The pioneering Ni- and Pd-dithiolate systems developed by Darensbourg provide a benchmark for completeness, but they offer no prospects to probe the effects of S-oxygenation at a variable ligand site. Analysis of the structural parameters of **1**−**4** reveals a systematic increase in the Ru−P bond distance as a function of S-oxygenation. This trend is reproduced computationally by density functional theory calculations providing insight into the potential of S-oxygenation to regulate substrate/product binding at the NHase active site.

(15) Lugo-Mas, P.; Dey, A.; Xu, L.; Davin, S. D.; Benedict, J.; Kaminsky, W.; Hodgson, K. O.; Hedman, B.; Solomon, E. I.; Kovacs, J. A. *J. Am. Chem. Soc.* **2006**, *128*, 11211–11221.
(16) Lugo-Mas, P.; Taylor, W.; Schweitzer, D.; Theisen, R. M.; Xu, L.; Shearer, J.; Swartz, R. D.; Gleaves, M. C.; DiPasquale, A.; Kaminsky, W.; Kovacs, J. A. *Inorg. Chem.* **2008**, *47*, 11228–11236.
(17) Heinrich, L.; Mary-Verla, A.; Li, Y.; Vaissermann, J.; Chottard, J. C. *Eur. J. Inorg. Chem.* **2001**, 2203–2206.
(18) Harrop, T. C.; Mascharak, P. K. *Acc. Chem. Res.* **2004**, *37*, 253–260.
(19) Harrop, T. C.; Olmstead, M. M.; Mascharak, P. K. *Inorg. Chem.* **2005**, *44*, 9527–9533.
(20) Rose, M. J.; Betterley, N. M.; Mascharak, P. K. *J. Am. Chem. Soc.* **2009**, *131*, 8340–8341.
(21) Rose, M. J.; Betterley, N. M.; Oliver, A. G.; Mascharak, P. K. *Inorg. Chem.* **2010**, *49*, 1854–1864.
(22) Yano, T.; Wasada-Tsutsui, Y.; Arii, H.; Yamaguchi, S.; Funahashi, Y.; Ozawa, T.; Masuda, H. *Inorg. Chem.* **2007**, *46*, 10345–10353.
(23) Farmer, P. J.; Solouki, T.; Mills, D. K.; Soma, T.; Russell, D. H.; Reibenspies, J. H.; Darensbourg, M. Y. *J. Am. Chem. Soc.* **1992**, *114*, 4601–4605.
(24) Mirza, S. A.; Pressler, M. A.; Kumar, M.; Day, R. O.; Maroney, M. J. *Inorg. Chem.* **1993**, *32*, 977–987.
(25) Farmer, P. J.; Verpeaux, J.-N.; Amatore, C.; Darensbourg, M. Y.; Musie, G. *J. Am. Chem. Soc.* **1994**, *116*, 9355–9356.
(26) Noveron, J. C.; Olmstead, M. M.; Mascharak, P. K. *J. Am. Chem. Soc.* **2001**, *123*, 3247–3259.
(27) Kaasjager, V. E.; Bouwman, E.; Gorter, S.; Reedijk, J.; Grapperhaus, C. A.; Reibenspies, J. H.; Smee, J. J.; Darensbourg, M. Y.; Derecskei-Kovacs, A.; Thomson, L. M. *Inorg. Chem.* **2002**, *41*, 1837–1844.
(28) Lee, C.-M.; Hsieh, C.-H.; Dutta, A.; Lee, G.-H.; Liaw, W.-F. *J. Am. Chem. Soc.* **2003**, *125*, 11492–11493.
(29) Galardon, E.; Giorgi, M.; Artaud, I. *Chem. Commun.* **2004**, 286–287.
(30) Chen, H.-W.; Lin, C.-W.; Chen, C.-C.; Yang, L.-B.; Chiang, M.-H.; Liaw, W.-F. *Inorg. Chem.* **2005**, *44*, 3226–3232.
(31) Lee, C.-M.; Chen, C.-H.; Chen, H.-W.; Hsu, J.-L.; Lee, G.-H.; Liaw, W.-F. *Inorg. Chem.* **2005**, *44*, 6670–6679.
(32) Chohan, B. S.; Maroney, M. J. *Inorg. Chem.* **2006**, *45*, 1906–1908.
(33) Grapperhaus, C. A.; Darensbourg, M. Y.; Sumner, L. W.; Russell, D. H. *J. Am. Chem. Soc.* **1996**, *118*, 1791–1792.
(34) Masitas, C. A.; Mashuta, M. S.; Grapperhaus, C. A. *Inorg. Chem.* **2010**, *49*, 5344–5346.
(35) Dilworth, J.; Zheng, Y.; Lu, S.; Wu, Q. *Transition Met. Chem.* **1992**, *17*, 364–368.
(36) Buonomo, R. M.; Font, I.; Maguire, M. J.; Reibenspies, J. H.; Tuntulani, T.; Darensbourg, M. Y. *J. Am. Chem. Soc.* **1995**, *117*, 963–973.
(37) Grapperhaus, C. A.; O'Toole, M. G.; Mashuta, M. S. *Inorg. Chem. Commun.* **2006**, *9*, 1204–1206.
(38) Buonomo, R. M.; Font, I.; Maguire, M. J.; Reibenspies, J. H.; Tuntulani, T.; Darensbourg, M. Y. *J. Am. Chem. Soc.* **1995**, *117*, 5427–5427.
(39) Tuntulani, T.; Musie, G.; Reibenspies, J. H.; Darensbourg, M. Y. *Inorg. Chem.* **1995**, *34*, 6279–6286.

Experimental Section

Materials and Methods. All reagents were obtained from commercially available sources and used as received unless otherwise noted. All solvents were dried and freshly distilled using standard techniques under a nitrogen atmosphere and degassed using freeze−pump−thaw techniques. Reactions were conducted using standard Schlenk techniques under an argon atmosphere or in an argon-filled glovebox unless otherwise noted. The complexes (bmmp-TASN)$RuPPh_3$, (**1**) and (bmmp-O_3-TASN)$RuPPh_3$, (**3**) were prepared as previously reported.[34]

(bmmp-O_2-TASN)$RuPPh_3$ (2). A suspension of **1** (128 mg, 0.18 mmol) was stirred in 50 mL of dry, degassed MeOH in a 250 mL Schlenk flask with a connected gas sample bulb with a precalibrated volume of 23 mL charged with O_2 (0.94 mmol) at a pressure of 1 atm. The flask containing **1** was evacuated just to the point of solvent boiling at which time the valve to the gas sample bulb was opened introducing the O_2. The solution was stirred for 5 min after which the solution was filtered to remove any trace solids followed by evacuation of the solvent. The crude product was dissolved in methanol. Slow evaporation of the solvent under air-free conditions yielded pure (**2**) as orange crystals. Yield: 93 mg (0.13 mmol, 72%). Electronic absorption (acetonitrile (22 °C)): λ_{max} (ε) 338 (1200), 385 (764). IR (KBr pellet), cm^{-1}: 30 58 (m), 2981 (br), 2961 (br), 2918 (br), 1948 (br), 1635(m), 1580 (s), 1489 (s), 1477 (s), 1458 (s), 1432 (s), 1139 (s), 1020 (s), 916 (s), 870 (s), 751 (s), 703 (s), 696 (s). (+)ESI-MS, m/z calcd for $C_{32}H_{43}N_2PRuS_3O_2$, $[M]^+$ 715.93 found, 715.69 Anal. Calcd for $C_{32}H_{43}N_2PRuS_3O_2$: C: 53.69%, H: 6.05%, N: 3.91% found C: 52.90%, H: 6.17%, N: 3.99%.

(bmmp-O_4-TASN)$RuPPh_3$ (4). A suspension of 50 mg (0.07 mmol) of **1** in 50 mL of dry, degassed MeOH was gently purged with O_2 for 2 h. The system was closed under an O_2 atmosphere and stirred for 120 h after which the solvent was removed under vacuum. The crude product was dissolved in water and filtered to remove insoluble products. Evaporation of the filtrate yields **4**. Yield: 15 mg (0.02 mmol, 30%). Electronic absorption IR (KBr pellet), cm^{-1}: 2970 (br), 2918 (br), 1948 (br), 1668 (s), 1580 (s), 1462 (s), 1437 (s), 1136(s), 1120 (s), 1029 (s), 1015 (s), 921 (s), 874 (s), 754 (s), 721 (s), 697 (s). (+)ESI-MS, m/z calcd for $C_{32}H_{43}N_2PRuS_3O_4$, $[M]^+$ 748.12 found, 748.12. Three attempts to obtain elemental analyses consistent with the ESI-MS were unsuccessful. This is ascribed to the partial degradation of **4** in water during isolation. The "best" analysis assumed Anal. Calcd for $C_{32}H_{43}N_2PRuS_3O_4 \cdot 0.5PPh_3$: C: 56.02%, H: 5.79%, N: 3.19% found C: 52.41%, H: 6.10%, N: 3.09%.

Physical Methods. Elemental analyses were obtained from Midwest Microlab (Indianapolis, IN). Infrared spectra were recorded on a Thermo Nicolet Avatar 360 spectrometer at 4 cm^{-1} resolution. ^1H NMR spectra were obtained on a Varian Inova 500 MHz spectrometer. Electrospray Ionization mass spectrometry (+ESI-MS) was performed by the Laboratory for Biological Mass Spectrometry at Texas A&M University. Cyclic voltammetry (CV) was performed using a PAR 273 potentiostat with a three electrode cell (glassy carbon working electrode, platinum wire counter electrode, and Ag pseudo reference electrode) at room temperature in an argon filled glovebox. All potentials were scaled to a ferrocene standard using an internal reference. Electronic absorption spectra were recorded with an Agilent 8453 diode array spectrometer with an air free 1 cm path length quartz cell.

Hydrolysis Trials. Hydrolysis of 4-nitrophenyl acetate: A mixture of **1** (5 mg, 7 μmol) and 4-nitrophenyl acetate (16 mg, 0.088 mmol) in MeOH/H_2O (8.2 mL/8.2 mL) and citrate buffer (1 M, pH = 4.8, 1.8 mL) was stirred at room temperature or 4 °C for 5 days. The reaction was monitored by UV−visible spectroscopy, and results were compared to a control sample with no added metal complex. The same method was applied to solutions containing **2** and **3**. Hydration of CH_3CN: A mixture of **1** (5 mg, 7 μmol) and 1,4-dimethoxybenzene (7 mg, 0.050 mmol) in CH_3CN (0.5 mL) and an HOAc/NaOAc (1 M, pH = 4.8, 0.5 mL) or PIPES (1 M, pH = 7.0, 0.5 mL) buffer was stirred at room temperature and at 4 °C for 5 days. After chloroform extraction, the organic soluble residue was dissolved in CD_3OD for ^1H and ^{13}C NMR analysis. The same procedure was applied to **2** and **3**.

Crystallographic Studies. An orange prism 0.25 × 0.16 × 0.12 mm^3 crystal of **2** was mounted on a glass fiber for collection of X-ray data on a Bruker SMART APEX CCD diffractometer. The SMART[40] software package (v 5.632) was used to acquire a total of 1,868 thirty-second frame ω-scan exposures of data at 100 K to a $2\theta_{max}$ = 56.22° using monochromated Mo Kα radiation (0.71073 Å) from a sealed tube and a monocapillary. Frame data were processed using SAINT[41] (v 6.45) to determine final unit cell parameters: a = 11.0203(7) Å, b = 17.4414(11) Å, c = 16.0538(10) Å, β = 96.4850(10)°, V = 3065.9(3) (19) $Å^3$, D_{calc} = 1.551 Mg/m^3, Z = 4 to produce raw *hkl* data that were then corrected for absorption (transmission min./max. = 0.90/0.93; μ = 0.802 mm^{-1}) using SADABS[42] (v 2.10). The structure was solved by Patterson methods in the space group $P2_1/n$ using SHELXS-90[43] and refined by least-squares methods on F^2 using SHELXL-97[44] incorporated into the SHELXTL[45] (v 6.14) suite of programs. All non-hydrogen atoms were refined with anisotropic atomic displacement parameters. Hydrogen atoms were placed in their geometrically generated positions and refined as a riding model. Methylene and phenyl H's were included as fixed contributions with $U(H)$ = $1.2U_{eq}$ (attached C atom) while methyl groups were allowed to ride (the torsion angle which defines its orientation was allowed to refine) on the attached C atom, and these atoms were assigned $U(H) = 1.5U_{eq}$. For all 7170 unique reflections (R(int) = 0.043) the final anisotropic full matrix least-squares refinement on F^2 for 374 variables converged at R1 = 0.035 and wR2 = 0.074 with a GOF of 1.05. Crystallographic parameters for **2** are displayed in Table 1.

Computational Methodology. Geometry optimization and subsequent molecular orbital (MO) analysis of complexes **1**−**4** were performed using the Gaussian 03 suite of programs. Density functional theory (DFT) calculations employed the BP86[46,47] and B3LYP[48−51] functionals. For these calculations, the LANL2DZ basis set was used for the Ru atom while the 6-31G(d) basis set was applied for all other atoms. Input coordinates for compounds **1**−**4** were taken from the crystallographic coordinates of **3** with the addition or abstraction of oxygen atoms as needed. Optimized coordinates are listed in Tables S1−S4 of the Supporting Information. Similar results were obtained with the BP86 and B3LYP functionals. The former provided a slightly better correlation with experimental bond distances and angles and was used for analyses of the frontier oribtals. Molecular

(40) *SMART* (v.5632); Bruker Advanced X-ray Solutions, Inc.: Madison, WI, 2005.
(41) *SAINT* (v6.45a); Bruker Advanced X-ray Solutions, Inc.: Madison, WI, 2003.
(42) *SADABS, Area Detector Absorption Correction* (v2.10); University Göttingen: Göttingen, Germany, 2003.
(43) Sheldrick, G. M. *Acta Crystallogr.* **1990**, *A46*, 467.
(44) *SHELXL-97, Program for the Refinement of Crystal Structures*; University Göttingen: Göttingen, Germany, 1997.
(45) *SHELXTL, Program Library for Structure Solution and Molecular Graphics* (v6.14); Bruker Advanced X-ray Solutions, Inc.: Madison, WI, 2000.
(46) Dey, A.; Chow, M.; Taniguchi, K.; Lugo-Mas, P.; Davin, S.; Maeda, M.; Kovacs, J. A.; Odaka, M.; Hodgson, K. O.; Hedman, B.; Solomon, E. I. *J. Am. Chem. Soc.* **2006**, *128*, 533–541.
(47) Dey, A.; Jeffrey, S. P.; Darensbourg, M.; Hodgson, K. O.; Hedman, B.; Solomon, E. I. *Inorg. Chem.* **2007**, *46*, 4989–4996.
(48) Boone, A. J.; Chang, C. H.; Greene, S. N.; Herz, T.; Richards, N. G. J. *Coord. Chem. Rev.* **2003**, *238−239*, 291–314.
(49) Hopmann, K. H.; Guo, J. D.; Himo, F. *Inorg. Chem.* **2007**, *46*, 4850–4856.
(50) Peplowski, L.; Kubiak, K.; Zelek, S.; Nowak, W. *Int. J. Quantum Chem.* **2008**, *108*, 161–179.
(51) Hopmann, K. H.; Himo, F. *Eur. J. Inorg. Chem.* **2008**, 1406–1412.

Table 1. Crystal Data and Structure Refinement for **2**

identification code	(bmmp-O_2-TASN)RuPPh$_3$
empirical formula	$C_{32}H_{43}N_2O_2PS_3Ru$
formula weight	715.90
temperature	100(2) K
wavelength	0.71073 Å
crystal system	monoclinic
space group	$P2_1/n$
unit cell dimensions	a = 11.0203(7) Å b = 17.4414(11) Å c = 16.0538(10) Å β = 96.4850(10)°
volume	3065.9(3) Å^3
Z	4
density (calculated)	1.551 Mg/m^3
absorption coefficient	0.802 mm^{-1}
F(000)	1488
crystal size	0.25 × 0.16 × 0.12 mm^3
θ range for data collection	1.73 to 28.11°
crystal color, habit	orange prism
index ranges	$-14 \le h \le 14$ $-23 \le k \le 22$ $-21 \le l \le 21$
reflections collected	26170
independent reflections	7170 [R(int) = 0.0432]
completeness to theta = 28.11°	95.6%
absorption correction	SADABS
max. and min transmission	0.897 and 0.932
refinement method	full-matrix least-squares on F^2
data/restraints/parameters	7170/0/374
goodness-of-fit on F^2	1.050
final R indices [$I > 2\sigma(I)$]	R1 = 0.0345, wR2 = 0.0712
R indices (all data)	R1 = 0.0416, wR2 = 0.0735
largest diff. peak and hole	0.941 and −0.533 e Å^{-3}

orbitals were visualized from cube files using the VMD software package.[52]

Results and Discussion

Synthesis and Characterization. Previously we reported the synthesis of (bmmp-TASN)RuPPh$_3$ (**1**) and its derivation under limiting dioxygen conditions to (bmmp-O_3-TASN)RuPPh$_3$ (**3**).[34] The sulfenato/sulfinato (RSO^-)/(RSO_2^-) donor set of **3** mimics the unusual post-translational modification of the NHase and SCNase active sites. The asymmetric sulfur−oxygenate **3** represents one of only three sulfenato/sulfinato derivatives prepared by direct reaction with dioxygen.[35,36] High yields of **3** were obtained by limiting the quantity (∼5 equiv) and duration (12 h) of dioxygen exposure. Monitoring the reaction by silica gel thin layer chromatography (TLC) revealed additional products. As outlined in Scheme 1, the oxygenation of **1** proceeds in a series of steps with distinct time frames. Immediately following O_2 exposure, the thiolato/sulfinato complex (bmmp-O_2-TASN)RuPPh$_3$ (**2**) is observed, R_f = 0.56, along with the thiolate precursor **1**, R_f = 0.68. After 5 min, **2** is the sole product and only traces of **1** are detected. Reaction times longer than 5 min yield a mixture of **2** and **3** (R_f = 0.45) yielding pure **3** after ∼15 min. From these results it can be inferred that **2** is a precursor to **3**. This is confirmed by the direct conversion of isolated **2** to **3** upon O_2 addition. Longer reaction times, 120 h, under limiting O_2 conditions yield the disulfinato complex (bmmp-O_4-TASN)RuPPh$_3$ (**4**), R_f = 0.2. Complex **4** can also be generated from isolated **3** or from **1** with excess O_2. In the presence of water, **4** degrades to the previously reported "intractable product" initially obtained in open-air oxygenation studies.[34]

The extent of S-oxygenation in complexes **2**−**4** was confirmed by +ESI-MS. Complex **2** displays a parent peak at m/z = 715.69 consistent with a theoretical value of 715.93 for [**2**]$^+$, Supporting Information, Figure S1. While +ESI-MS typically yields [M+H]$^+$ or [M+Na]$^+$ ions, the direct oxidation of neutral species at the probe tip to yield [M]$^{\cdot+}$ is known for easily oxidized samples such as **1**−**4**.[53] Samples of **2** prepared with $^{18}O_2$ show the expected shift to m/z = 720.13 confirming O_2 as the source of both O-atoms in the product, Supporting Information, Figure S2. The mixed sulfenato/sulfinato complex **3** displays a peak at m/z = 731.11 that shifts to 737.13 when the sample is prepared with $^{18}O_2$.[34] The +ESI-MS of the disulfinato complex **4** has only small intensity at the theoretical value of m/z = 748.12. A larger peak at m/z = 485.64 associated with PPh$_3$ dissociation is observed along with free PPh$_3$ at m/z = 262.30, Supporting Information, Figure S3. While the +ESI-MS reveals the number of O-atoms in **2**−**4**, it does not provide information on their positions. This can be readily assigned by infrared spectroscopy. The infrared spectra of **2** and **4** display intense sulfinate stretching bands similar to **3**. The asymmetric and symmetric SO_2 stretches of **3** at 1137 and 1020 cm^{-1} were confirmed by isotopic labeling studies.[34] Complex **2** displays intense bands at 1139 and 1020 cm^{-1}, Supporting Information, Figure S4. The bis-sulfinato complex **4** displays two sets of stretches at 1136, 1120, 1029, and 1015 cm^{-1}, Supporting Information, Figure S4. The energies of the sulfinato stretches in **1**−**4** are similar to those reported by Darensbourg et al. in their complete series of nickel sulfur oxygenates.[36]

Voltammetric studies of **1**−**3** were conducted in acetonitrile solution with 0.1 M tetrabutylammonium hexafluorophosphate (TBAHFP) as supporting electrolyte. All potentials are referenced to the ferrocenium/ferrocene (Fc^+/Fc) couple. The square wave voltammograms, Figure 2, clearly delineate the changes in the Ru$^{III/II}$ reduction potential as a function of sulfur oxygenation. The Ru(II)-dithiolato precursor **1** displays a Ru$^{III/II}$ redox couple with $E_{1/2}$ = −851 mV. Oxygenation of **1** to **2** stabilizes the lower oxidation because of electron withdrawing effects of the two O atoms. The $E_{1/2}$ of **2** is shifted by +458 mV with respect to **1** resulting in a Ru$^{III/II}$ potential of −393 mV. The shift is similar to that observed upon oxygenation of other Ru thiolates.[54] The $E_{1/2}$ of **3**, −263 mV, reflects an additional shift of +130 mV as compared to **2** as another O-atom is added. The cathodic shift for a single sulfenato O-atom is less than half of the shift induced by the two O-atoms of the sulfinate as previously noted by Darensbourg et al.[36] The reversibility of each redox event was established by cyclic voltammetry, Supporting Information, Figures S5−S7. Each complex displays a quasi-reversible Ru$^{III/II}$ couple with ΔE values of 109, 73, and 79 mV for **1**, **2**, and **3** at a scan rate of 200 mV/s.

(52) Humphrey, W.; Dalke, A.; Schulten, K. *J. Mol. Graphics* **1996**, *14.1*, 33–38.

(53) Henderson, W.; McIndoe, J. S. In *Mass Spectrometry of Inorganic, Coordination and Organometallic Compounds*; Wiley: Hoboken, NJ, 2005; pp 47−105.

(54) Grapperhaus, C. A.; Poturovic, S.; Mashuta, M. S. *Inorg. Chem.* **2005**, *44*, 8185–8187.

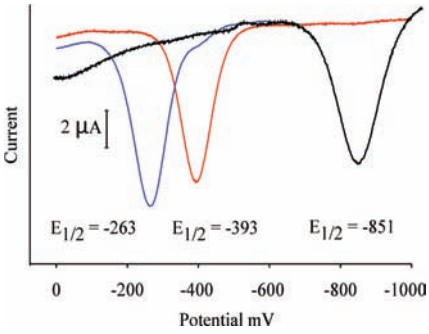

Figure 2. Squarewave voltammograms of **1** (black), **2** (red), and **3** (blue) in acetonitrile with 0.1 TBAHFP as supporting electrolyte. Potentials referenced to Fc^+/Fc.

The solution properties of **1**− **4** were investigated to probe for potential hydrolytic activity.[55] Metal complex promoted hydrolysis requires dissociation of the phosphine to provide an open coordination site for substrate binding or direct participation of the S-oxygenate moieties in the hydrolysis.[17] Structural studies (vide infra) reveal an increased Ru−P bond distance as a function of S-oxygenation suggesting the phosphine may become labile in solution generating a transient five-coordinate intermediate. Solutions of **2** and **3** in 1:1:1 mixture of acetonitrile, methanol, and PIPES buffer (pH = 7.0) yield small quantities of acetamide after stirring under inert conditions for 5 days. The identity of the acetamide was confirmed by ^1H and ^{13}C NMR, Supporting Information, Figures S8−S11, following evaporation of solvent and extraction of soluble products into $CDCl_3$. Attempts to quantify acetamide using 1,4-dimethoxybenzene as an internal standard yielded inconsistent results.[17] In all cases, the acetamide integration was significantly greater than the standard, but proportional to free PPh_3. Since PPh_3 originates from **2** and **3** upon dissociation, these peak ratios suggest a stoichiometric reaction. No acetamide is observed for **1** under identical conditions. In buffered aqueous mixtures at pH = 4.8, complexes **1**−**3** displayed no hydrolytic activity. The lack of activity for **1** suggests the phosphine remains coordinated to the kinetically inert Ru(II) under the conditions tested. In contrast, the acetonitrile hydrolysis activity of **2** and **3** is consistent with partial PPh_3 dissociation in solution. It should be noted that exchange inert Co(III) sulfenato complexes have been reported to hydrolyze nitriles via a ligand-centered mechanism in buffers at pH = 4.8.[17] However, under these conditions no hydrolysis was observed for **1**−**3**. Further studies are underway to exchange the coordinated phosphine for more labile ligands. Complex **4** degraded to an intractable orange product upon the addition of water precluding catalytic attempts.

Structural Characterizations. Orange block shaped crystals of **2** in the monoclinic space group $P2_1/n$ were obtained upon slow evaporation of methanol solutions of the complex under air free conditions. Crystal data and structure refinement details are listed in Table 1. Complex **2** contains a six-coordinate ruthenium(II) ion in an N_2S_3P donor set with one thioether (S1), one sulfinato (S2), and one thiolato (S3) sulfur donor, Figure 3. The TASN ligand backbone (N1, N2, S1) occupies one face of a

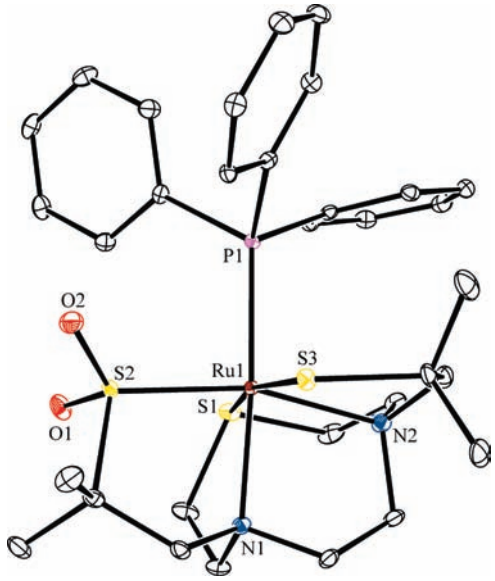

Figure 3. ORTEP representation of **2** showing 40% probability ellipsoids. Hydrogen atoms have been omitted to clearly illustrate the oxygenation of S2.

distorted octahedron. The three sulfur donors are arranged in a meridional fashion as in other six-coordinate bmmp-TASN based complexes.[9,10,12] The sulfinato sulfur S2 of **2** sits trans to the amine N2 in the same position as in **3**.[34] The thiolato sulfur S3 of **2** occupies the position trans to the thioether S1. This is the same position as the sulfenate in **3** consistent with a stepwise progression of **1** to **2** to **3** upon O_2 exposure.

Comparison of the structure of **2** with previously reported crystallographic data for **1** and **3** reveals significant distinctions as a function of sulfur oxygenation. Selected bond distances for **1**−**3** listed in Table 2. The $Ru-S_{sulfinato}$ distances of 2.2473(6) and 2.2548(9) Å in **2** and **3** are 0.158(1) and 0.151(1) Å, respectively, shorter than the corresponding $Ru-S_{thiolato}$ distance in **1**. Similarly, the $Ru-S_{thiolato}$ distances of **2** and **1**, 2.3943(6) and 2.3754(10) Å, are 0.045(1) and 0.026(1) Å, respectively, longer than corresponding $Ru-S_{sulfenato}$ bond length in **3**. As noted previously, sulfur−oxygenation of a metal coordinated thiolate eliminates a four electron $d\pi-p\pi$ antibonding interaction between the metal and the sulfur.[15,47,56−58] Additionally, oxidation of the sulfur decreases its ionic radius. The net result is a decreased Ru−S bond distance.[57] Further, the loss of π-donating ability induced by S-oxygenation increases metal−ligand bond distances with traditional π-acceptors. The Ru−P bond distance consistently increases from 2.2911(10) to 2.3519(6) to 2.3790(9) Å for **1**, **2**, and **3**, respectively. The same trend is noted in the $Ru-S_{thioether}$ bond distances.

Computational Investigations. Geometry optimization and subsequent molecular orbital (MO) analysis of complexes **1**−**4** were performed using the BP86 functional with the LANL2DZ basis set for Ru and the 6-31G(d)

(55) Chin, J. *Acc. Chem. Res.* **1991**, *24*, 145–152.

(56) Farmer, P. J.; Reibenspies, J. H.; Lindahl, P. A.; Darensbourg, M. Y. *J. Am. Chem. Soc.* **1993**, *115*, 4665–4674.

(57) Grapperhaus, C. A.; Darensbourg, M. Y. *Acc. Chem. Res.* **1998**, *31*, 451–459.

(58) Grapperhaus, C. A.; Mullins, C. S.; Kozlowski, P. M.; Mashuta, M. S. *Inorg. Chem.* **2004**, *43*, 2859–2866.

Table 2. Selected Experimental and Computational (BP86/LANL2DZ+6-31G(d)) Bond Distances (Å) and Angles (deg) for **1**−**4**

	1		**2**		**3**		**4**
	experimental	calculated	experimental	calculated	experimental	calculated	calculated
Ru1−S1	2.2900(10)	2.3395	2.3102(6)	2.3641	2.3622(9)	2.4323	2.4052
Ru1−S2	2.4057(9)	2.4443	2.2473(6)	2.3273	2.2548(9)	2.3361	2.3476
Ru1−S3	2.3754(10)	2.4401	2.3943(6)	2.4387	2.3493(9)	2.3941	2.3826
Ru1−P1	2.2911(10)	2.3248	2.3519(6)	2.3811	2.3790(9)	2.4105	2.4496
Ru1−N1	2.198(2)	2.2518	2.1927(19)	2.2603	2.178(3)	2.2392	2.2574
Ru1−N2	2.178(2)	2.2288	2.200(2)	2.2670	2.192(3)	2.2614	2.2815
S2−O1			1.4906(17)	1.5329	1.489(3)	1.5317	1.5344
S2−O2			1.4658(18)	1.5133	1.471(3)	1.5148	1.5102
S3−O3					1.556(3)	1.5755	1.5312
S3−O4							1.5055
P1−Ru−S2	95.44(2)	91.20	93.16(2)	93.43	90.72(3)	92.50	93.91
P1−Ru−S3	92.42(3)	93.34	93.99(2)	93.29	91.59(3)	91.10	94.06
S2−Ru−S3	94.93(3)	95.61	97.09(2)	97.81	94.13(3)	96.42	98.52

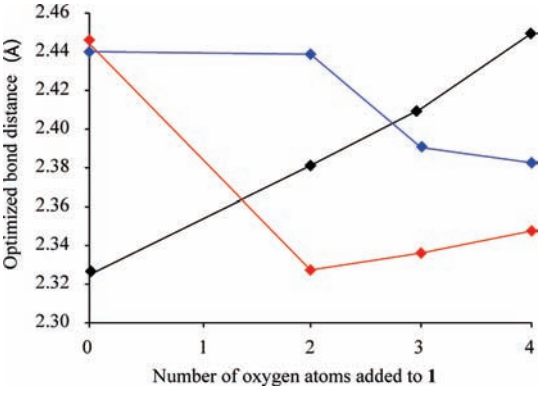

Figure 4. Plot of optimized (BP86/LANLDZ+6-31G(d)) Ru−L bond distance versus number of oxygen atoms in **1**−**4**. Ru−P (black), Ru−S2 (red), Ru−S3 (blue).

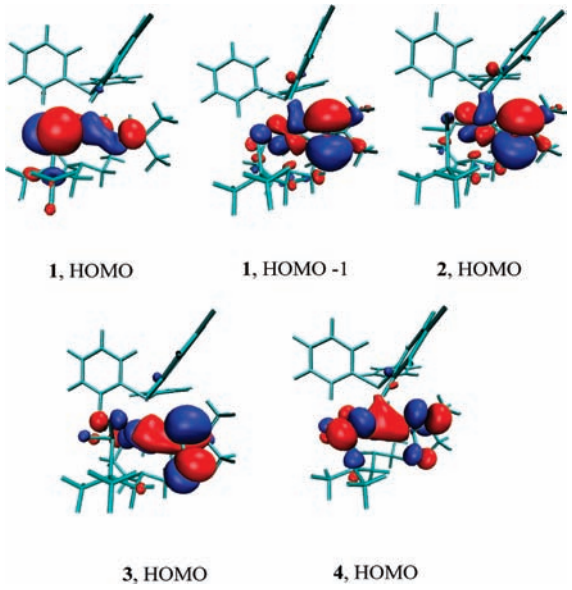

Figure 5. Isosurface plot (isovalue = 0.03) of the highest occupied molecular orbital (HOMO) of **1**−**4** and the HOMO-1 of **1** based on BP86/LANLDZ+6-31G(d) calculations.

basis set for all other atoms. The calculated metal−ligand bond distances accurately reproduce the experimental values for complexes **1**−**3** within 0.02 to 0.08 Å, Table 2. Although no experimental data is available for **4**, the optimized bond distances are consistent with the trends observed for **1**−**3**, Figure 4. Calculated bond angles reproduce experimental values within 4°, Table 2. Similar results were obtained when the B3LYP functional was used.

The optimized metal ligand distances reflect changes in the electronic structure as a function of sulfur oxygenation. As shown in Figure 4, the effects of sulfur oxygenation in the series **1**−**4** are revealed by the Ru−S2, Ru−S3, and Ru−P bond distances. As expected, large changes in Ru−S bond distances occur upon oxygenation of the sulfur donor. A decrease of 0.12 Å in the Ru−S2 bond distance occurs when S2 is oxygenated from a thiolate in **1** to a sulfinate in **2**. The Ru−S2 bond distance then only slightly increases in **3** and **4**. The largest decrease in the Ru−S3 bond distance, 0.04 Å, is observed when the thiolate of **2** is oxidized to a sulfenate in **3**. Only small changes are observed between the S3-thiolates of **1** and **2** and the S3-oxygenates of **3** and **4**. While changes in the Ru−S bond distances reflect bonding changes at that specific atom, the Ru−P bond distance consistently increases with each subsequent O-atom added to the sulfur donors. As shown in Figure 4, there is a direct correlation between the Ru−P bond distance and the level of sulfur oxygenation. The data fits a straight line according to the equation $y = 2.331 + (0.040)x$ ($R^2 = 0.98$), where y is the Ru−P bond distance in Å and x is the number of O-atoms added to sulfur. For the bis-sulfinato complex **4**, the theoretical bond length increases to 2.450 Å. The elongation of the Ru−P bond as a function of sulfur oxygenation supports the suggestion that post translational modifications in NHase or SCNase regulates substrate/product binding.

Analysis of the frontier orbitals of **1**−**4** shows a direct connection between sulfur oxygenation and changes in the Ru−P bonding. In **1**, the occupied frontier molecular orbitals are dominated by metal−sulfur interactions as observed in other metal−thiolates.[12,47,58−61] The highest occupied molecular orbital (HOMO) and HOMO-1, Figure 5, show π* interactions between filled "t_{2g}" orbitals on the metal and p-type lone pairs on the sulfur on S2 and S3, respectively. Additionally, the HOMO-1 includes

(59) Bellefeuille, J. A.; Grapperhaus, C. A.; Derecskei-Kovacs, A.; Reibenspies, J. H.; Darensbourg, M. Y. *Inorg. Chim. Acta* **2000**, *300*, 73–81.
(60) Chang, C. H.; Boone, A. J.; Bartlett, R. J.; Richards, N. G. J. *Inorg. Chem.* **2003**, *43*, 458–472.
(61) Kennepohl, P.; Neese, F.; Schweitzer, D.; Jackson, H. L.; Kovacs, J. A.; Solomon, E. I. *Inorg. Chem.* **2005**, *44*, 1826–1836.

a significant σ-bonding interaction between metal-centered orbital and the phosphine ligand that strengthens the Ru−P bond. This σ-bonding interaction can be considered as an "outlet" for the 4 electron dπ−pπ repulsion described for "t_{2g}-rich" metal−thiolates. A similar σ-donation is observed in the HOMO between the metal and the thioether sulfur S1, with an additional polarization of the metal orbital toward the phosphine donor. In **2**, one of the thiolates, S2, has been oxygenated and no longer participates in π-bonding/antibonding with Ru. The HOMO of **2** is localized on the remaining thiolate, S3, and Ru. The HOMO of **2** is similar to the HOMO-1 of **1** with a π^* interaction between Ru and S and a strong σ-bonding interaction between Ru and P. Complexes **3** and **4** lack thiolate donors and do not show the same type of interactions as **1** and **2**. Rather, the HOMOs of **3** and **4** are dominated by S−O π^* interactions that are σ-bonding with respect to the metal sulfur−oxygenate bond. As in the HOMO of **1**, the metal centered orbital is slightly polarized toward the phosphine ligand. Overall, Ru−S interactions reinforce the Ru−P bond through the HOMO and HOMO-1 of **1** and the HOMO of **2**. The Ru−P bond is only weakly affected by Ru−S interactions in the HOMOs of **3** and **4**.

Summary and Conclusions. A family of sulfur oxygenated derivatives has been prepared through the controlled oxygenation of **1** under limiting O_2 conditions. The key synthetic features of our approach include restricted quantities of O_2 and short reaction times. Prior studies were largely conducted open to air or in oxygen saturated solutions under an O_2 atmosphere for hours or days. By fixing the quantity of O_2 and the duration of the reaction, conditions were optimized to reproducibly obtain high yields of **2**, **3**, or **4** without the need for O-atom transfer reagents or purification by column chromatography.

The S-oxygenation of **1** proceeds in a series of stepwise additions. Rapid addition of O_2 to **1** yields **2**. This step is promoted by the t_{2g}^6 electron configuration of Ru(II). As reported previously, the π and π^* interactions between thiolato sulfur donors and t_{2g}-rich metal ions increase the covalency of the metal−sulfur bond and promote sulfur oxygenation.[12] The second oxygenation step, **2** to **3**, proceeds significantly more slowly than the first. This is attributable, at least in part, to steric interactions between the remaining thiolate and PPh_3.[34] Further oxygenation of **3** to **4** is further hindered by the PPh_3 and occurs only on longer time scales. Each S-oxygenate, **2**−**4**, is stable in acetonitrile and methanol solutions in the absence of O_2. Complex **4** degrades in the presence of water.

The N_2S_3 donor set of bmmp-TASN has been employed to model the protein derived donors at active sites of NHase and SCNase. As in the enzymes, ligand coordination positions two reactive thiolate donors on the same octahedral face as a sixth, variable ligand. The t_{2g}^6 electron configuration of Ru(II) in **1**−**4** reproduces key electronic features of the low-spin t_{2g}^5 and t_{2g}^6 configurations of Fe(III) and Co(III) at the enzyme active sites. Further, as noted in the current study, the Ru−S π^* interactions stabilizes Ru−P σ-bonding. Upon oxygenation, the Ru−S π^* interaction is relieved, weakening the Ru−P bond as evidenced by the direct correlation between the oxygenation level and Ru−P bond distance. Notably, this increase in bond length correlates with the stoichiometric hydrolysis of acetonitrile by **2** and **3**. It is expected that the same M−L bond distance trend would be observed for Fe(III) and Co(III). In support of this, Mascharak et al. have shown that S-oxygenation of an iron-thiolate facilitates photodissociation of NO.[21] Our series of complexes confirms the observation for that isolated example to show a direct correlation between the number of O-atoms and the M−L bond distance. These results are consistent with the notion that sulfur oxygenation increases substrate/product lability and hydrolytic activity at the NHase and SCNase active sites.

Acknowledgment. Acknowledgment is made to the National Science Foundation (CHE-0749965) for funding. M.S.M. thanks the Department of Energy, Grant DE-FG02-08CH11538, and the Kentucky Research Challenge Trust Fund for upgrade of our X-ray facilities.

Supporting Information Available: +ESI-MS and FT-IR spectra of **2** and **4** and cyclic voltammograms of **1**−**3** in PDF format and crystallographic data in CIF format (CCDC 780375). This material is available free of charge via the Internet at http://pubs.acs.org.